In: Stilla U, Rottensteiner F, Paparoditis N (Eds) CMRT09. IAPRS, Vol. XXXVIII, Part 3/W4 --- Paris, France, 3-4 September, 2009

RAY TRACING AND SAR-TOMOGRAPHY FOR 3D ANALYSIS OF MICROWAVE SCATTERING AT MAN-MADE OBJECTS

S. Auer [a], X. Zhu [a], S. Hinz [b], R. Bamler [ac]

[a] Remote Sensing Technology, Technische Universität München, Arcisstrasse 21, 80333 München - (Stefan.Auer, Xiaoxiang.Zhu)@bv.tum.de
[b] Institute for Photogrammetry and Remote Sensing, Universität Karlsruhe, Kaiserstrasse 12, 76128 Karlsruhe - stefan.hinz@ipf.uni-karlsruhe.de
[c] Remote Sensing Technology Institute, German Aerospace Center (DLR), Münchner Strasse 20, 82234 Oberpfaffenhofen-Wessling - Richard.Bamler@dlr.de

Commission VI, WG VI/4

KEY WORDS: SAR Simulation, Ray Tracing, POV Ray, SAR Tomography, TerraSAR-X

ABSTRACT:

An inherent drawback of SAR imaging of complex 3D structures is the potential layover of more than one scatterer in one resolution cell. Such scatterers can be separated by tomographic processing of multiple SAR images acquired with different across-track baselines. Simulation tools may further support interpretation of such layover effects appearing in multi-body urban scenes. In this paper, an existing 2D simulation approach, developed for separating different kinds of reflection effects in the azimuth-range plane, is enhanced by including the elevation direction as third dimension and thus enabling the comparison of the SAR simulation results with 3D imaging techniques such as tomography. After introducing the simulation concept, tools for three-dimensional analysis of scattering effects are presented. Finally, simulated data are compared with real elevation data extracted from TerraSAR-X images for showing potential fields of application.

1. INTRODUCTION

High resolution SAR sensors like TerraSAR-X or Cosmo-SkyMed provide SAR images having a resolution of below one meter in spotlight mode. While in SAR images of coarse resolution several dominant scatterers from man-made objects at slightly different ranges may be condensed into a single pixel, these will be separable in high resolution images. Hence, more image features can be distinguished due to an increased number of deterministic effects and due to an increased signal to clutter ratio for dominant scatterers (Adam et al., 2008).

However, visual interpretation of image features in high resolution SAR images remains challenging due to range dependent geometrical effects. SAR maps the 3D world basically into a cylindrical coordinate system, where range and azimuth are the image coordinates and elevation is the coordinate, along which all scattering contributions are integrated, i.e. all scatterers are mapped into the same resolution cell in the azimuth-range plane if they have the same spatial distance with respect to the SAR sensor. Access to the third coordinate, elevation, is achieved by multi-baseline methods, like Persistent Scatterer Interferometry (Ferretti et al., 2001; Kampes, 2006) or SAR tomography (Reigber & Moreira, 2000; Fornaro et al, 2003; Zhu et al., 2008).

Simulation of scattering effects for urban areas may support visual interpretation of high resolution SAR images. In this context, Franceschetti and co-workers (Franceschetti et al., 1995) distinguish between two different kinds of SAR simulators: image simulators and SAR raw data simulators. In the past, different concepts have been presented for simulating artificial SAR images for urban areas (Balz, 2006; Mametsa et al., 2001) and for simulating SAR raw data by illuminating simplified building models (Franceschetti et al., 2003).

The simulator presented in this paper applies ray tracing algorithms and has been developed for simulating artificial SAR reflectivity maps (Auer et al., 2008). The approach is focused on geometrical correctness while physical effects and speckle effects are neglected. In addition to a reflectivity map containing all backscattered intensities, reflection effects are assigned to different image layers based on available bounce level information, i.e. separate layers for single bounce, double bounce, etc. Hence, interpretation of deterministic reflection phenomena appearing at man-made objects is simplified.

So far, for providing image data in azimuth and range, two out of three dimensions of the imaging system have been exploited. The novelty of the presented approach compared to other simulation concepts relates to the fact that the complete 3D geometry of the SAR imaging process is simulated and stored. This enables one, based on the simulated 2D SAR, to retrieve information about the existence of multiple scatterers in one resolution cell in the SAR image. We show that simulation of the distribution of point scatterers in elevation direction may support the interpretation of estimated elevation coordinates derived by SAR Tomography.

The structure of the paper is organized as follows. Firstly, the basic simulation concept is introduced in Section 2 where four major parts of the simulation concept are explained including necessary developments for extraction and analysis of elevation data. Simulation results displaying elevation data are compared with real data extracted from a TerraSAR-X image in Section 3. Finally, in Section 4, a short summary is given and future work is addressed.

2. SIMULATION CONCEPT

The simulation approach presented in this paper is based on ray tracing algorithms provided by POV Ray (Persistence of Vision Ray Tracer), a free-ware ray tracing software. Main advantages of POV Ray are free access to its source code, optimized processing time, separability of multiple reflections and existing interfaces to common 3D model formats. In order to provide necessary output data for two-dimensional analysis of reflection phenomena, additional parts have been included to POV Ray's source code. The simulation concept consists of four major parts:

- Modeling of scene objects (Section 2.1)
- Sampling of the 3D model scene in POV Ray (Section 2.2)
- Creation of reflectivity maps (Section 2.3)
- 3D analysis of reflection effects by means of output data provided by POV Ray (Section 2.4)

In the following subsections, the processing chain will be explained in more detail.

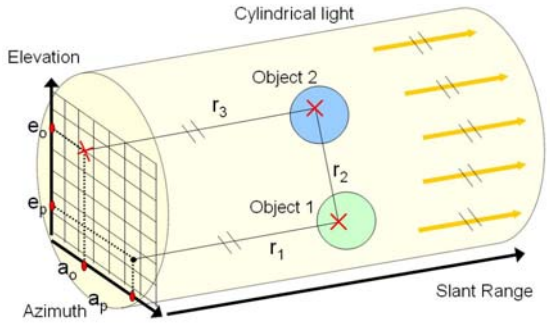

Figure 1: Approximation of SAR system by a cylindrical light source and an orthographic camera; 3D sampling due to coordinates in azimuth, slant-range, and elevation

2.1 Modeling of scene objects

First, the 3D scene to be illuminated by the virtual SAR sensor has to be described in the modeling step. 3D models can be designed in POV Ray or can be imported into the POV Ray environment. Then, parameters are adapted for describing the reflection behavior at object surfaces. To this end, POV Ray offers parametric models for specular reflection and diffuse reflection. A reflectivity factor for each surface defines the loss of intensity affecting rays specularly reflected at object surfaces.
In the case of a modeled SAR system both the light source and the camera are located at the same position in space. The concept for approximating the imaging geometry of the SAR system is shown in Figure 1. Focusing effects due to SAR processing in azimuth and range are considered by using a cylindrical light source and an orthographic camera whose image plane is hit perpendicularly by incoming signals.

2.2 Sampling of the 3D model scene

For analyzing backscattered signals within the modeled 3D scene, rays are followed in reverse direction starting at the center of an image pixel and ending at the ray's origin at the light source (Whitted, 1980). This concept is commonly referred to as Backwards Ray Tracing (Glassner, 2002). Since ray tracing is performed for each pixel of the image plane, output data for creating reflectivity maps is derived by discrete sampling of the three-dimensional object scene (Auer et al., 2008).
Coordinates in azimuth and range are derived by using depth information in slant-range provided during the sampling step. For instance, according to Figure 1, focused azimuth coordinates a_f and slant-range coordinates r_f of double bounce contributions are calculated by:

$$a_f = \frac{a_0 + a_p}{2} \quad (1)$$

$$r_f = \frac{r_1 + r_2 + r_3}{2} \quad (2)$$

where a_0, a_p = azimuth coordinates of the ray's origin and the ray's destination at the image plane

r_1, r_2, r_3 = depth values derived while tracing the ray through the 3D model scene

So far, only two axes of the three-dimensional imaging system - azimuth and range - have been used for reflection analysis (Auer et al., 2008). However, the third dimension, elevation, may provide potential to enhance the simulators capacities to 3D analysis of reflection effects. To this end, extraction of elevation data has been added to the sampling step. According to the imaging concept shown in Figure 1, the elevation coordinate for a double bounce contribution is derived by means of the following equation:

$$e_f = \frac{e_0 + e_p}{2} \quad (3)$$

where e_0, e_p = elevation coordinates of the ray's origin and the ray's destination at the image plane

At this point, elevation data derived during the sampling step shall be discussed in more detail. Due to Eq. (3) and the discrete sampling of the scene, all backscattering objects are assumed to behave as point scatterers. Resolution in elevation is not affected by limits occurring due to the size of sampling intervals along the elevation direction or the length of the elevation aperture (Nannini et al., 2008). From a physical point of view, deriving discrete points directly in elevation direction may be a disadvantage since comparison of the processed reflectivity function with a simulated one could be a desirable task. For instance, in the case of single bounce, the discrete concept will not be able to represent a planar surface continuously but only by discrete points.
For layover caused by multiple reflections along the elevation direction the discrete simulation concept is nonetheless reasonable since approaches for tomographic analysis also seek for scatterers whose backscattered intensity is concentrated in individual points along the elevation direction. Concentration on scene and SAR geometry and thereby neglecting the physical characteristics provides some advantages, though, to overcome well known limitations of tomographic analysis (Zhu et al., 2008). For instance, it leads to a better understanding of the SAR geometry in the elevation direction by means of simulating the reflectivity slice which is helpful for 3D reconstruction. Additionally, it has the potential to provide the number of scatterers in a cell as a priori for parametric tomographic estimators if the scene geometry is available at a very detailed level, e.g. based on airborne LIDAR surface models.

Eventually, the simulation process provides the following output data for each reflection contribution detected in the 3D object scene:

- coordinates in azimuth, slant range, and elevation [units: meter]
- intensity data [dimensionless value between 0 and 1]
- bounce level information for every reflection contribution [1 for single bounce, 2 for double bounce, etc.]
- flags marking specular reflection effects [value 0 or 1]

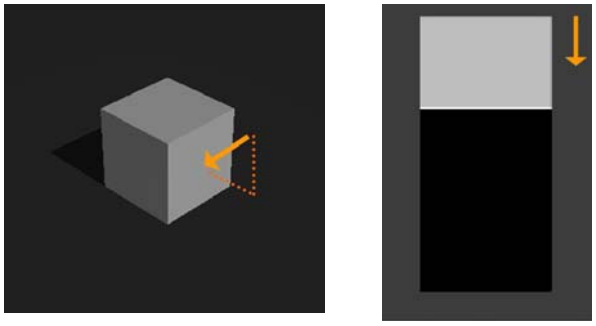

Figure 2: left: Simulation using box model having a size of 20 m x 20 m x 20 m, line of sight indicated by arrow; right: simulated reflectivity map simulated (slant-range indicated by arrow)

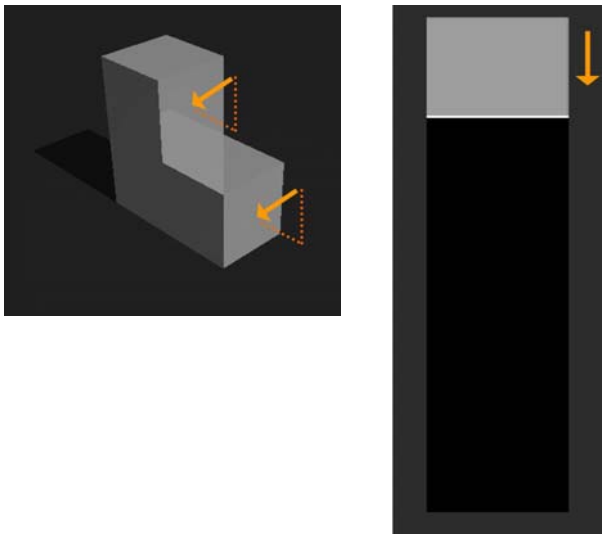

Figure 3: simulation using step model (left), line of sight indicated by arrow; simulated reflectivity map (right), slant-range indicated by arrow

2.3 Reflectivity maps in azimuth and slant range

Firstly, all reflection contributions are mapped into the azimuth – slant range plane. Afterwards, a regular grid is imposed onto the plane and intensity contributions are summed up for each image pixel. Figure 2 shows the resulting reflectivity map for a cube (dimensions: 20 m x 20 m x 20 m) which has been illuminated by the virtual SAR sensor using an incidence angle of 45 degrees. The size of one resolution cell has been fixed to cover 0.5 m x 0.5 m in azimuth and slant range. Surface parameters are chosen in a way that box surfaces can be clearly distinguished from ground parts, i.e. in the current example box surfaces show stronger diffuse backscattering than the surrounding ground. Following top-down in ground range direction, diffuse single bounce contributions of the ground are visible followed by a layover area of ground, wall of the box and top of the box. At the end of the layover area, a strong double bounce line is visible which is caused by the interaction between the front wall and the ground in front of the box.
For this type of scene geometry, a 2D simulation and analysis is usually sufficient. The next section will however illustrate examples that underline the necessity of including the elevation direction as third dimension into the simulation.

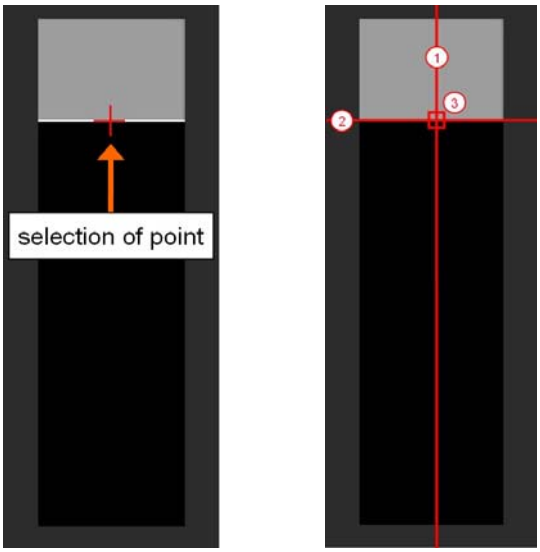

Figure 4: selection of pixel for elevation analysis (left); definition of three slices (right) in slant-range (1), azimuth (2), and elevation direction (3)

2.4 3D analysis of scattering effects

Figure 3 shows a reflectivity map simulated by illuminating a step model (width: 10 m, length 20 m, height 20 m). For providing the map, the same imaging geometry has been chosen as for the box example, i.e. the step was oriented in direction to the sensor and the incidence angle was fixed to 45 degrees in order to obtain specific overlay effects for single and double bounce contributions which are explained in the following. Compared to the reflectivity map containing the box model (Figure 2), the reflectivity map of the step shows similar characteristics. Both the layover area of single bounce contributions and the location of focused double bounce contributions are identical. Only the size of the shadow zone indicates a height difference between the illuminated objects. In the case of the step model, separation of dihedrals – two right angles at the steps – is impossible in the reflectivity map since all double bounce effects are condensed in one single line.
Hence, separation of scattering effects in elevation direction may be helpful since it enables to resolve layover effects for the purpose of distinguishing several scatterers within one resolution cell. To this end, an interactive click-tool has been included into the simulator for defining two-dimensional slices to be analyzed. In the case of the given reflectivity map for the step model, one pixel is selected, e.g. located in the double bounce area as shown in Figure 4. Based on the coordinates of the pixel center, three slices are defined:

- slice no. 1 for displaying elevation data in slant-range direction
- slice no. 2 for displaying elevation data in azimuth direction

- slice no. 3 for displaying intensities in elevation direction

According to the defined slices, necessary data in slant-range, azimuth and elevation are extracted out of the data pool provided by the sampling process in POV Ray.

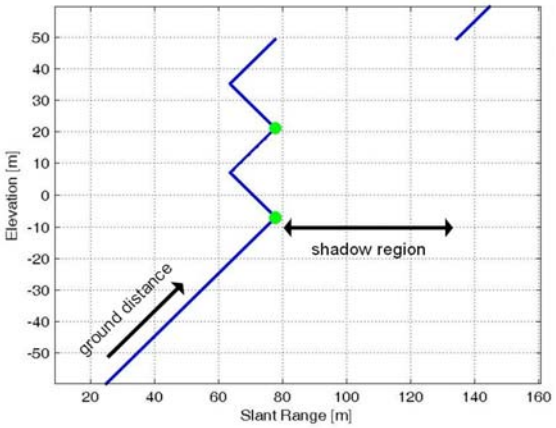

Figure 5: Slice 1: elevation heights in slant-range direction (slice 1 in Figure 4 corresponds to slant range interval 60 m to 140 m); blue: single bounce contributions, green: double bounce contributions

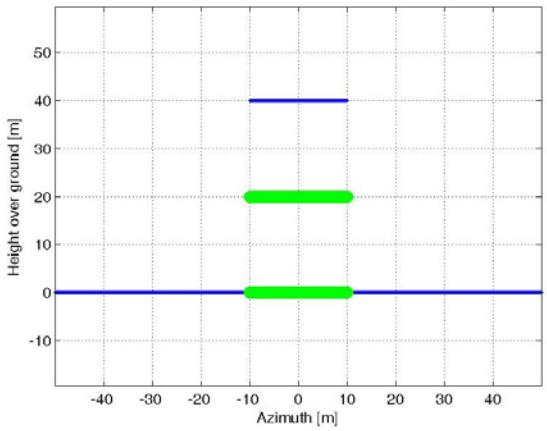

Figure 6: Slice 2: elevation information along azimuth direction displayed in height over ground; blue: single bounce contributions, green: double bounce contributions; zero level = level of ground surrounding the step

Since the incidence angle used for sampling the 3D model scene is known, slice no. 1 pointing in slant range direction can be presented by two versions, either by displaying elevation heights (Figure 5), i.e. elevation coordinates with respect to a master height situated in the center of the image plane used for sampling the scene, or by providing height information in height over ground geometry, i.e. heights with respect to the ground surrounding the box.
Following the slant-range direction from left to right, displaying height data in elevation heights enables to distinguish between range intervals containing one scatterer and areas containing several scatterers resulting in layover effects, which can not be separated in reflectivity maps such as shown in Fig. 3 (right). In Figure 5, reflection caused by direct backscattering are colored in blue color while double bounce contributions are indicated by green spots. Due to the incidence angle of 45 degrees, double bounce effects are focused at the same position in slant-range and are overlaid by both single bounce contributions at the ground and single bounce contributions reflected at the end of the step up-side.
Following slice no. 2 along its way, elevation information is shown along the azimuth direction in height over ground (Figure 6). After passing an interval of contributions directly backscattered at the ground, the layover region starts showing the width of the double bounce areas in azimuth, which are equal to the width of the step model. As expected, double bounce contributions caused by the interaction between perpendicular faces are concentrated at the corresponding intersection lines and, hence, show a height value of 0 and 20 meters, respectively.

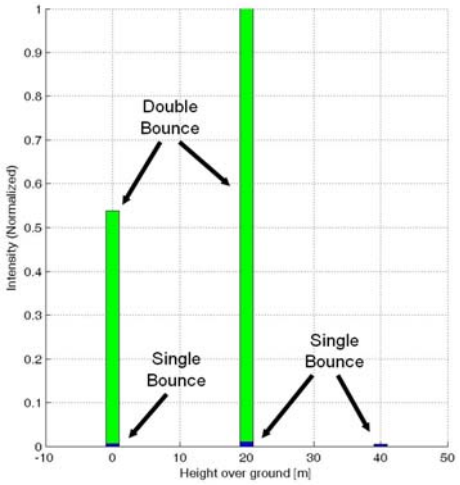

Figure 7: Slice 3: normalized intensities along elevation direction; step width in elevation: 2 meters; blue: single bounce contributions, green: double bounce contribution

Slice no. 3 pointing in elevation direction is shown in Figure 7. After the spatial sampling along elevation direction is chosen by the operator, intensity contributions are assigned to elevation intervals and summed up. Since the selected pixel is located within the double bounce area of two dihedrals, slice no. 3 shows two strong double bounce contributions caused by the interaction of step faces (colored in green) accompanied by weak direct backscattering derived at the step faces (colored in blue). Although the radiometric quality of detected intensity contributions is moderate due to simplified reflection models and the approximation of SAR signals by rays, proportions between single and double bounce intensities within one resolution cell are well represented.
In the following Section, simulation results will be compared to real data derived by tomographic analysis.

3. COMPARISON: SIMULATION VS. REAL DATA

For demonstrating potential applications of SAR simulation in elevation dimension, a practical example extracted from tomographic analysis using TerraSAR-X high resolution spotlight data is provided in this section and compared to simulation results.

3.1 Object modelling

Fig.8 shows the 2D intensity map for the convention center of Las Vegas acquired by TerraSAR-X. For the purpose of this paper, an azimuth-range pixel marked by a green dot has been taken as example. The complex valued measurement at this pixel corresponds to the integration of the reflected radar signal

along the elevation direction. It is located at the layover area. Fig.9 gives a closer look to the ground truth at that area. The left image shows the convention center visualized in Google Earth in which the pixel of interest is included in the area marked by a red block. The right image tells that the returns from the roof of the convention center and from the plaza near ground mainly contribute to the measurement of this pixel.

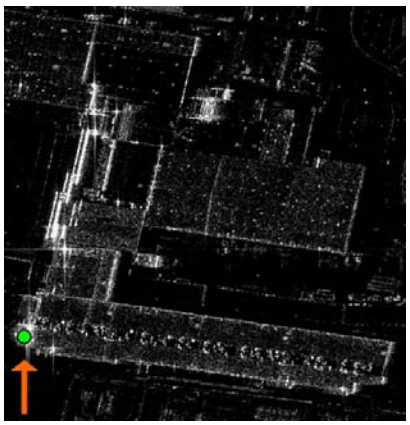

Figure 8: TerraSAR-X intensity image of convention center, Las Vegas; selected pixel marked by green spot

Figure 9: corresponding aerial image, © Google Earth

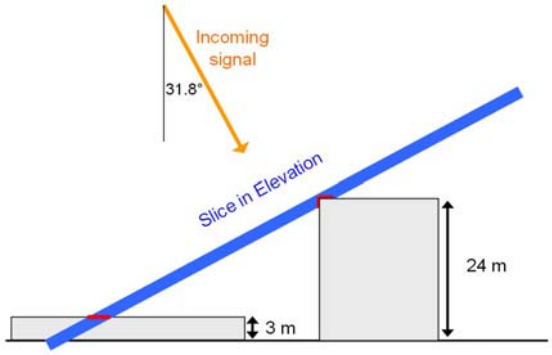

Figure 10: Model of the ground truth for the pixel of interest

For simulation, we simplify the ground truth to the following model as depicted in Fig. 10. The incidence angle for the acquisition is adapted to the real SAR acquisition and, hence, is 31.8 degrees. The taller building refers to the convention center which has a height of about 24m, while the lower building stands for the plaza near ground. Heights are measured over ground. The measurement for the pixel of interest refers to the integral of the returns from the objects included in the strip highlighted in blue color. For simulation purposes, two box models are used for modeling both the plaza and the convention center (Figure 11). The roughness of the plaza's surface is assumed to be slightly higher than the roughness of walls and roof parts of the convention center.

3.2 Simulation vs. real data

The reflectivity profile of the resolution cell along elevation direction is derived using the simulation concept described in Section 2. Pixel selection is adapted to extracted real data as shown in Figure 8. Afterwards, the resulting slice in elevation is displayed in height over ground geometry (Figure 12). Heights of reflecting objects are reliably extracted as two single bounce contributions at heights of 3 and 24 meters.

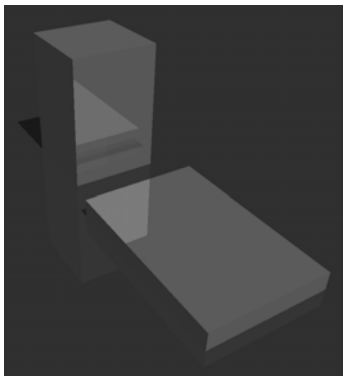

Figure 11: 3D model scene containing two boxes for approximating layover effect (flat box: 20 m x 30 m x 3 m; tall box: 15 m x 15 m x 24 m); diffuse backscattering behaviour at all box surfaces

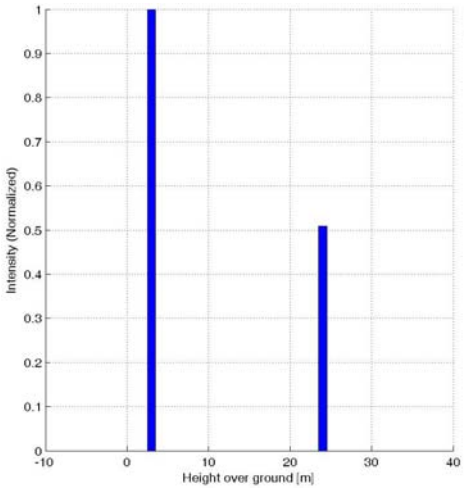

Figure 12: discrete elevation coordinates for backscattering objects; step-width in elevation: 1 meter

Fig. 13 shows the result of tomographic analysis for the corresponding position in real TerraSAR-X data. The reflection profile has been calculated with the approach described in (Zhu et al., 2008). As input data, 16 TerraSAR-X spotlight images with an across-track baseline range of 270m have been used. The peaks in reflection profile show nice correspondence with the simulated results, which underlines the accurate geometric properties of the simulation. However, it has to be noted that accurate estimation of intensity proportions is not possible as ground truth for surface properties was not available. At this point, simulated intensity values only indicate a stronger diffuse backscattering from the plaza which is also visible in the reflectivity map extracted from real SAR data. Enhanced information about the scattering behaviour of the plaza and the convention center may enable better simulation results in the

future. To not only compare the position of the peaks but also the shape of the reflection profile, the elevations of the simulated point scatterers (see Fig.12) were fed into the tomographic analysis assuming the same imaging configuration as for the real TerraSAR-X data. As can be seen from Fig. 14, the profile matches very well with the tomographic results from real data (Fig. 13). This example provides a validation of the SAR simulator in the third dimension by comparing to the tomographic analysis result using the TerraSAR-X data. In a further step, it can also be used for validation of tomographic algorithms by simulating the complex valued measurements of a data stack with different baseline distributions.

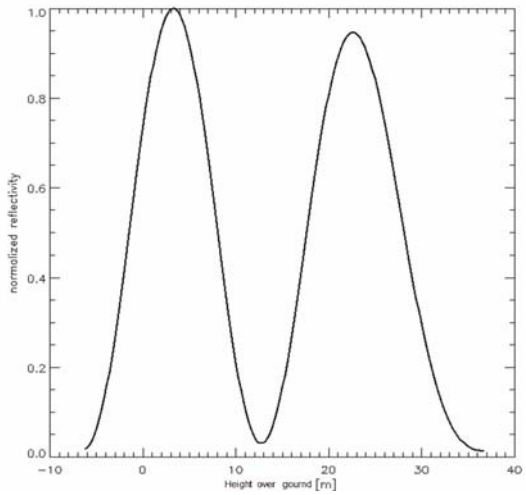

Figure 13: reflectivity function extracted from TerraSAR-X data by SAR-Tomography; intensity peaks estimated at heights of 3 m and 22.5 m

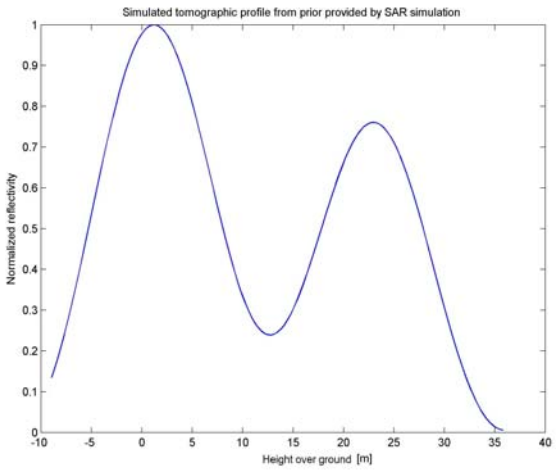

Figure 14: reflectivity function estimated from simulated data extracted from simulator by SAR-Tomography.

4. SUMMARY AND OUTLOOK

In this paper, a concept and its prototype implementation for 3D analysis of reflection effects has been presented. 3D model scenes are sampled by ray tracing techniques for providing necessary output data in azimuth, slant-range and elevation. Elevation slices are determined by pixel selection in reflectivity maps in the azimuth-range plane. Comparison of simulated data with real SAR data for a selected urban scene provided promising results. Further studies will have to show whether simulated elevation data may also support the geometrical analysis of more complex 3D urban scenes since visual interpretation of the simulation results is expected to become more complicated due to the increased number of visible building features. Meanwhile, the SAR estimator will be extended for the purpose of validation of tomographic algorithms.

5. REFERENCES

Adam, N.; Eineder, M.; Yague-Martinez, N.; Bamler, R., 2008. High Resolution Interferometric Stacking with TerraSAR-X. *Proceedings of IGARSS 08*, Boston, USA

Auer, S.; Hinz, S.; Bamler, R., 2008. Ray Tracing for Simulating Reflection Phenomena in SAR Images. *Proceedings of IGARSS 08*, Boston, USA

Balz, T. 2006. Real-Time SAR Simulation of Complex Scenes Using Programmable Graphics Processing Units. *Proceedings of the ISPRS TCVII Mid-term Symposium*

Ferretti, A.; Prati, C.; Rocca, F, 2001. Permanent scatterers in SAR interferometry. *IEEE Transactions on Geoscience and Remote Sensing, 39*, 8-20

Fornaro, G.; Serafino, F.; Soldovieri, F., 2003. Three-dimensional focusing with multipass SAR data. *IEEE Transactions on Geoscience and Remote Sensing, 41*, 507-517

Franceschetti, G.; Iodice, A.; Riccio, D.; Ruello, G., 2003. SAR raw signal simulation for urban structures. *IEEE Transactions on Geoscience and Remote Sensing, 41*, 1986-1995

Franceschetti, G.; Migliaccio, M.; Riccio, D., 1995. The SAR simulation: an overview. *Geoscience and Remote Sensing Symposium, 1995. IGARSS '95. 'Quantitative Remote Sensing for Science and Applications', International, 3*, 2283-2285 vol.3

Glassner, A. S., 2002. *An Introduction to Ray Tracing*. Morgan Kaufmann, 329

Kampes, B. M., 2006. *Radar Interferometry - Persistent Scatterer Technique*. Springer, 213

Mametsa, H. J.; Rouas, F.; Berges, A.; Latger, J, 2001. Imaging Radar simulation in realistic environment using shooting and bouncing rays technique. *Proceedings of SPIE: 4543. SAR Image Analysis, Modeling and Techniques IV, Toulouse*

Nannini, M.; Scheiber, R.; Moreira, A., 2008. On the Minimum Number of Tracks for SAR Tomography. *Proceedings of IGARSS 08*, Boston, USA

Reigber, A.; Moreira, A., 2000. First demonstration of airborne SAR tomography using multibaseline L-band data. *IEEE Transactions on Geoscience and Remote Sensing, 38*, 2142-2152

Whitted, T., 1980. An improved illumination model for shaded display. *Commun. ACM, 23*, 343-349

Zhu, X.; Adam, N.; Bamler, R., 2008. First Demonstration of Space-borne High Resolution SAR Tomography in Urban Environment Using TerraSAR-X Data. *Proceedings of CEOS SAR Workshop on Calibration and Validation*